nature neuroscience

A neural mechanism for exacerbation of headache by light

Rodrigo Noseda[1], Vanessa Kainz[1], Moshe Jakubowski[1], Joshua J Gooley[2], Clifford B Saper[2,3], Kathleen Digre[4] & Rami Burstein[1,3]

The perception of migraine headache, which is mediated by nociceptive signals transmitted from the cranial dura mater to the brain, is uniquely exacerbated by exposure to light. We found that exacerbation of migraine headache by light is prevalent among blind individuals who maintain non–image-forming photoregulation in the face of massive rod/cone degeneration. Using single-unit recording and neural tract tracing in the rat, we identified dura-sensitive neurons in the posterior thalamus whose activity was distinctly modulated by light and whose axons projected extensively across layers I–V of somatosensory, visual and associative cortices. The cell bodies and dendrites of such dura/light-sensitive neurons were apposed by axons originating from retinal ganglion cells (RGCs), predominantly from intrinsically photosensitive RGCs, the principle conduit of non–image-forming photoregulation. We propose that photoregulation of migraine headache is exerted by a non–image-forming retinal pathway that modulates the activity of dura-sensitive thalamocortical neurons.

Migraine is a recurring, episodic neurological disorder characterized as unilateral, throbbing headache that is commonly associated with a variety of other symptoms (for example, nausea, vomiting, irritability and fatigue)[1,2]. Migraine pain is thought to originate from chemical irritation of the meninges, which leads to transmission of nociceptive signals from the dura mater to the brain via the so-called trigeminovascular pathway[3]. The first- and second-order neurons in this pathway are, respectively, sensory neurons in the trigeminal ganglion that project centrally to the spinal trigeminal nucleus (SpV)[4] and dura-sensitive neurons in laminae I and V of SpV that project to the posterior thalamus[5]. Prolonged neuronal activation during a migraine attack is thought to induce peripheral and central sensitization along the trigeminovascular pathway, which stands to explain the throbbing headache[6], accompanying scalp and neck-muscle tenderness[7], and whole-body cutaneous allodynia[8].

The perception of migraine headache is uniquely exacerbated during exposure to ambient light as compared with the pain level felt in the dark[9,10]. Other forms of abnormal light sensitivity, commonly referred to as photophobia, are typically associated with anterior segments disorders of the eye such as uvetis, cyclitis, iritis and blepharitis[11], and intracranial pathologies such as meningitis, subdural hemorrhage and intracranial tumors[9,12–14]. Unlike forms of photophobia defined as abnormal light sensitivity[11] or ocular discomfort induced by light (also termed photo-oculodynia)[15], we postulated that exacerbation of migraine headache by light[10,16] is driven by photic signals transmitted from the retina via the optic nerve to central neurons that process nociceptive signals from the meninges.

Retinal projections to the brain constitute image-forming and non–image-forming pathways. Image formation in vertebrates, the tracking and interpreting of visual objects and patterns, is generated primarily by photoactivation of the classic opsin-based photopigments of retinal rods and cones, and subsequent activation of RGCs, whose axons project to visual cortices via the optic nerve, the lateral geniculate nucleus and the superior colliculus. Non–image-forming functions in vertebrates, including the entrainment of the biological clock to the dark-light cycle, adaptation of pupillary size to light[17] and suppression of melatonin release by light[18], are all mediated by a specialized pathway originating from intrinsically photosensitive RGCs (ipRGCs), whose axons project via the optic nerve to the suprachiasmatic nucleus (SCN), intergeniculate leaflet (IGL) and olivary pretectal nucleus (OPT)[17,19–25]. Activation of ipRGCs is achieved not only extrinsically by rods and cones but also intrinsically by virtue of their unique photopigment, melanopsin[20,26–30].

The neural mechanism for the photic exacerbation of migraine headache is unknown. Also unknown is whether central trigeminovascular neurons can be modulated, either directly or indirectly, by photic signals from the retina. We found that exacerbation of headache by light was preserved in blind migraineurs that rely primarily on non–image-forming photoreception but was absent in those who lost their optic nerve or the eyes. We also found that light modulated the activity of a subset of trigeminovascular thalamic neurons that receive input from the retina and project to multiple cortical areas.

RESULTS

Photophobia in blind individuals suffering from migraine

The prevalence of migraine-associated photophobia was documented in 20 blind individuals suffering from migraine (15 females, 5 males). Their demographic profile was similar to that of migraineurs with

Departments of [1]Anesthesia and [2]Neurology, Beth Israel Deaconess Medical Center, and [3]Program in Neuroscience, Harvard Medical School, Boston, Massachusetts, USA. [4]Department of Neurology and Ophthalmology, Moran Eye Center, University of Utah, Salt Lake City, Utah, USA. Correspondence should be addressed to R.B. (rburstei@bidmc.harvard.edu).

Received 26 August 2009; accepted 23 November 2009; published online 10 January 2010; doi:10.1038/nn.2475

Table 1 Incidence of photosensitivity during migraine in blind persons

Diagnosis	Eyeballs	PLR	Sleep cycle	Manifestation of photosensitivity		Migraine with aura	Age	Age at first attack	Migraine (d per month)
				Migraine free	During migraine				
Without light perception (n = 6)									
Retinal prematurity	Enucleated	–	Irregular	None	None	No	51	7	1
Retinal prematurity, secondary glaucoma	Enucleated	–	Fragmented	None	None	No	56	22	8
Retinal cancer	Enucleated	–	Fragmented	None	None	No	34	32	3
Congenital syphilis, secondary glaucoma	Enucleated	–	Fragmented	None	None	No	55	13	1
Bilateral optic neuropathy	Present	No	Fragmented	None	None	Yes	41	37	2
Posterior ischemic optic neuropathy	Present	n/a	Fragmented	None	None	Yes	71	18	4
With light perception (n = 14)									
Retinitis pigmentosa	Present	Yes	Regular	None	Headache ↑	No	57	3	0.5
Retinitis pigmentosa	Present	Yes	Fragmented	Unpleasant	Headache ↑	Yes	41	12	12
Leber's congenital amaurosis	Present	Yes	Regular	Unpleasant	Headache ↑	Yes	43	22	6
Leber's congenital amaurosis	Present	Yes	Regular	None	Headache ↑	No	21	3	5
Cones/rods dystrophy	Present	Yes	Regular	Unpleasant	Headache ↑	No	39	7	2
Cones/rods dystrophy	Present	Yes	Regular	None	Headache ↑	No	17	12	2
Cones/rods dystrophy	Present	Yes	Regular	None	Headache ↑	No	19	6	8
Retinal degeneration	Present	n/a	Fragmented	Unpleasant	Headache ↑	Yes	55	30	4
Retinal prematurity	Present	n/a	Regular	Ocular pain	Headache ↑	No	28	25	1
Retinal prematurity	Present	Yes	Fragmented	None	Headache ↑	No	55	8	1
Retinal prematurity	Present	Yes	Regular	None	Headache ↑	Yes	29	8	30
Bilateral optic neuropathy	Present	Yes	Regular	None	Headache ↑	No	60	50	4
Bilateral retinal detachment and glaucoma	Present	Yes	Regular	Ocular pain	Headache ↑	Yes	45	7	4
Posterior ischemic optic neuropathy	Present	Yes	Regular	None	Headache ↑	No	54	33	30

n/a, not available.

normal eyesight in terms of age (43.5 ± 3.4 years, mean ± s.e.m.), age at the time of first migraine attack (17.8 ± 2.9), years of migraine history (25.8 ± 3.8), frequency of attacks (6.4 ± 1.9 per month) and incidence of visual aura (35% of patients).

Six of the patients had no light perception as a result of bilateral enucleation of the eyes, or damage to the optic nerves (**Table 1**). Surgical eye removal was carried out because of retinal detachment caused by retinal prematurity resulting from neonatal overexposure to oxygen (two cases), retinal cancer (one case) or congenital syphilis/secondary glaucoma (one case). Optic nerve lesions were caused by bilateral optic neuropathy (one case) or extensive hemorrhage (one case). As with mice lacking rods, cones and melanopsin[30], these individuals suffered irregular or fragmented sleep pattern and exhibited deficient pupillary light response (PLR). The intensity of their headaches were unaffected by light, suggesting that migraine photophobia depends on signals relayed from the retina to the brain via the optic nerve.

Of the blind individuals that suffered from migraine, 14 were capable of detecting light in the face of markedly deficient image-forming perception (<20/200 vision, <10° visual field). Eight individuals were diagnosed with inherited retinal degeneration (retinitis pigmentosa, Leber's congenital amaurosis or cone-rod dystrophy), three had retinal detachment due to neonatal overexposure to oxygen (retinopathy of prematurity) and the remaining three were diagnosed with bilateral optic neuropathy, bilateral retinal detachment and glaucoma, or shock optic neuropathy after a large hemorrhage (**Table 1**). Using interviews, medical records or direct examination, we found that most of these individuals had normal PLR and regular sleep pattern (in three cases, sleep pattern was disrupted and PLR data were unavailable). In this group, migraine headache intensity under ambient light was rated 9.2 ± 0.2 on a 0–10 subjective scale, compared with 6.2 ± 0.3 in a dim or dark environment. The preservation of migraine photophobia in the face of rod/cone degeneration led us to investigate whether central trigeminovascular neurons can be regulated by non–image-forming signals from the eye.

Anterograde tracing of RGC projections to the thalamus

We previously mapped retinal projections to non–image-forming brain areas in the rat using intravitreal injections of cholera toxin subunit B (CTB) or recombinant adeno-associated virus containing a green fluorescent protein reporter gene (rAAV-GFP)[22]. Using immunostained brain sections from those experiments, we searched for retinal axons in brain areas containing dura-sensitive neurons, including the SpV, parabrachial nucleus, posterior thalamic nuclear group and ventral posteromedial thalamic nucleus[31–33]. Among these, only the dorsocaudal region of the posterior thalamic nuclear group (mostly contralateral to the injected eye) contained anterograde-labeled retinal axons (**Fig. 1**). Viewed in a parasagittal plane (**Supplementary Fig. 1**), fibers labeled by intravitreal injection of 1% CTB (wt/vol) descended ventrorostrally from the main visual pathway toward the dorsal aspect of the posterior thalamic nuclear group, between the anterior pretectal and the lateral posterior thalamic nuclei.

We examined retinal input into posterior thalamic nuclear group in nine rats that received large intravitreal injections of rAAV-GFP (1.7×10^{10} viral particles in 10 µl) and in three rats that received a smaller amount of the tracer (8.5×10^{9} particles in 5 µl). Axonal labeling in the caudal portion of the posterior thalamus was examined in a series of coronal sections stretching about 1 mm rostro-caudally (−3.7 to −4.5 mm from bregma; **Fig. 1**). The larger injection of the tracer produced heavy axonal labeling in the optic tract and the main visual thalamic nuclei, including all subdivisions of the lateral geniculate nucleus and the brachium superior colliculus (**Fig. 1a**). The smaller injection of the tracer, however, yielded heavy axonal labeling

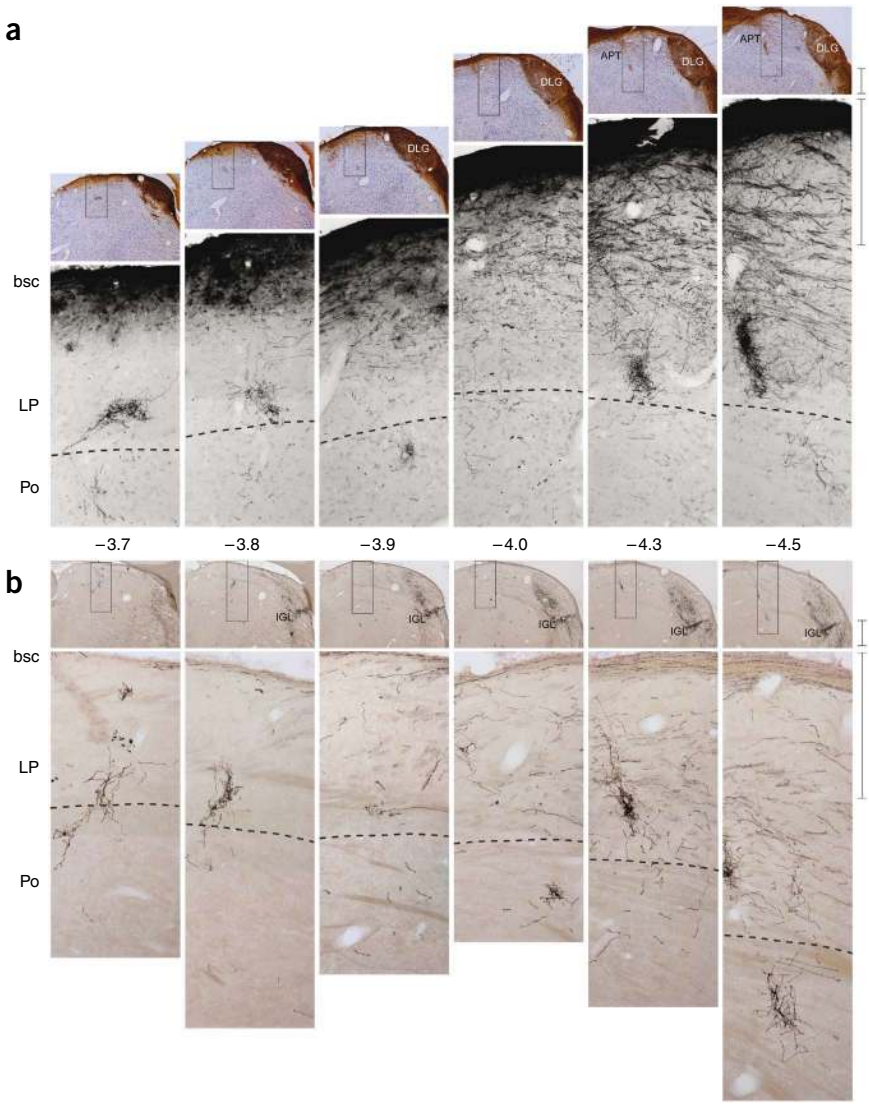

Figure 1 Projections of RGCs to the lateral posterior thalamic nuclei (LP) and posterior thalamic nuclear group (Po). (**a**,**b**) Anterograde tracing of retinal afferents was performed using large (**a**) or small (**b**) injections of rAAV-GFP into the vitreous body of the eye. (**a**) Top, low-power images of coronal sections counterstained with thionin showing immunolabeled retinal afferents (brown) in the main visual pathway. Bottom, high-power detail of the boxed areas in the corresponding top panels showing retinal afferents in ventral lateral posterior thalamic nuclei and dorsal posterior thalamic nuclear group. These images show only the blue channel, which isolated the labeled fibers from the background Nissl staining. (**b**) Top, low-power images of coronal sections showing preferential labeling of retinal afferents in the IGL. Bottom, high-power detail of the boxed areas in the corresponding top panels showing immunolabeled retinal afferents in ventral lateral posterior thalamic nuclei and dorsal posterior thalamic nuclear group. Preferential labeling of non–image-forming pathways by the smaller rAAV-GFP injection (**b**) compared with the larger injection (**a**) reflected preferential labeling of ipRGCs. Note that the retinal afferents ran dorsoventrally from the main visual pathway through ventral aspect of lateral posterior thalamic nuclei and into dorsal aspect of posterior thalamic nuclear group (**a**,**b**). Note that the density of labeled axons in ventral lateral posterior thalamic nuclei and dorsal posterior thalamic nuclear group was similar between **a** and **b**, suggesting that most labeled axons in these areas were of ipRGC origin. Numbers indicate distance from bregma (mm). APT, anterior pretectal nucleus; bsc, brachium superior colliculus; DLG, dorsal part of lateral geniculate nucleus. Scale bars represent 500 μm.

primarily in the IGL (**Fig. 1b**) and OPT, reflecting preferential uptake by ipRGCs[22]. Despite these marked differences, both methods of injection yielded similar patterns and density of labeled axons in the ventral part of lateral posterior thalamic nuclei and the dorsal part of posterior thalamic nuclear group (**Fig. 1** and **Supplementary Fig. 2**).

Injection of the retrograde tracer Fluorogold into the posterior thalamic nuclear group resulted in simultaneous labeling of cell bodies in laminae I and V of the contralateral SpV and RGCs, including melanopsinergic ipRGCs, in the contralateral eye (**Supplementary Figs. 3** and **4**). We therefore set out to search for individual thalamic neurons that process and integrate nociceptive signals from the meninges (mediated by trigeminovascular SpV neurons) and photic signals from the eye.

Effects of light on dura-sensitive thalamic neurons

Using extracellular single-unit recording in deeply anesthetized rats, we identified 20 units in the posterior thalamus that responded to stimulation of the dura (**Fig. 2a**,**b** and **Supplementary Fig. 5**), 14 of which were also photosensitive. Compared with their ongoing activity in the dark, the mean firing rate of the 20 dura-sensitive units increased about twofold in response to ambient fluorescence light (500 lx) and fourfold in response to bright light (50,000 lx) shone directly on the contralateral eye (**Fig. 2c**). As a control, we studied 14 units that were unresponsive to stimulation of the dura; these units were also unresponsive to ambient light (**Fig. 2c**). Histological analysis of the recording sites indicated that most dura/light-sensitive neurons (9 of 13) were localized at or above the dorsal border of the posterior thalamic nuclear group (**Fig. 2d**,**e**). Dura-sensitive units that were unresponsive to light were found more ventrally in posterior thalamic nuclear group proper, as well as in the ventral posteromedial thalamic nucleus and the ventral posterolateral thalamic nucleus (**Fig. 2d**,**e**). Control units, which were neither dura sensitive nor light sensitive, were present in all of these regions (**Fig. 2d**,**e**).

Latencies of neuronal photoactivation were measured using three levels of illuminance. Illuminance of the contralateral eye with 50,000 lx induced delayed activation in seven units (3-, 4.4-, 5-, 5-, 6-, 20-, 24-s latencies; **Fig. 2f**) and rapid activation in another set of seven units (<1 s; **Fig. 2g**). Binocular ambient illuminance with 3,000 lx induced delayed activation in five units (2-, 20-, 200-, 200- and 280-s latencies; **Fig. 2h**) and rapid activation (<1 s) in two units that were tested repeatedly (**Fig. 2i**); the latter latencies averaged 295 ± 66 ms in one unit (nine trials ranging 48–619 ms) and 426 ± 141 ms in the other (five trials ranging 243–983 ms). Ambient illuminance with 500 lx (ceiling fixtures of fluorescent light) induced delayed activation in four units (170-, 190-, 210- and 340-s latencies; **Fig. 2j**) and rapid

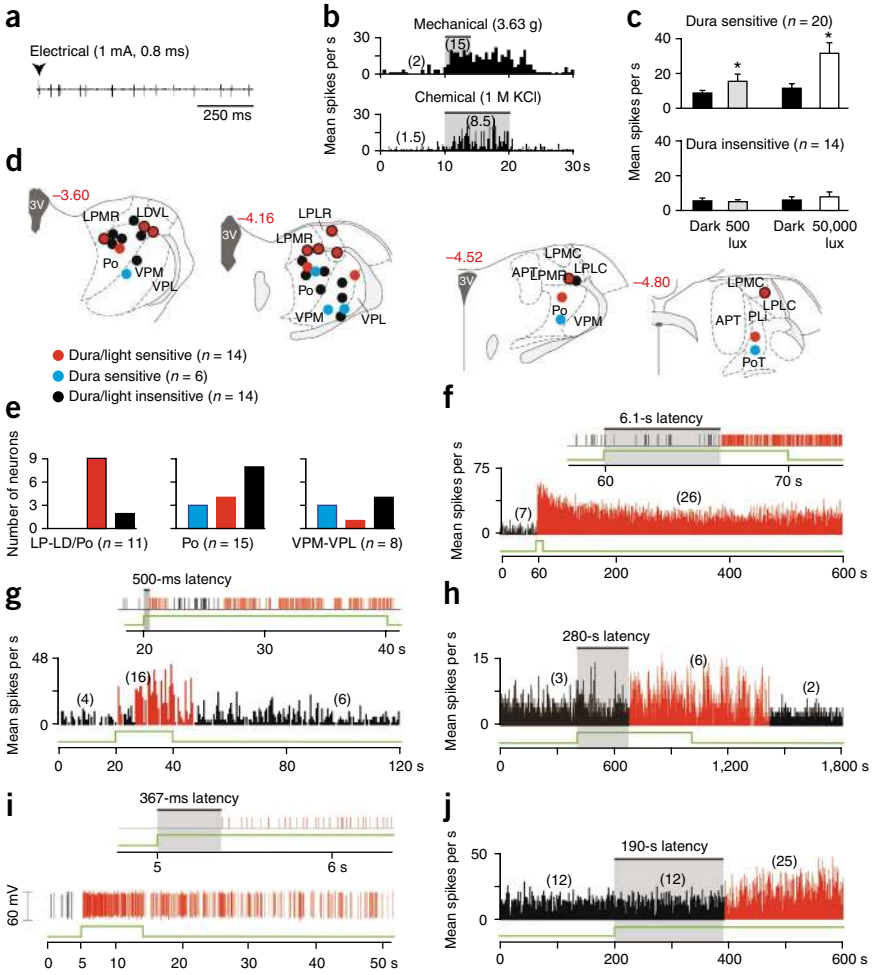

Figure 2 Photosensitivity of dura-sensitive thalamic neurons. (**a**,**b**) Identifying neuronal responses to electrical (**a**), mechanical and chemical (**b**) stimulation of the dura. (**c**) Effects of ambient light (500 lx) and bright light (50,000 lx) on firing rate (mean ± s.e.m.) of dura-sensitive versus dura-insensitive thalamic neurons (* $P < 0.05$, Wilcoxon matched-pairs signed-ranks test). (**d**) Histological localization of the recorded neurons. Drawings and numbers indicating distance from Bregma (mm) are from ref. 46. LDVL, laterodorsal thalamic nucleus, ventrolateral; LPLC, lateral posterior thalamic nucleus, laterocaudal; LPLR, lateral posterior thalamic nucleus, laterorostral; LPMC, lateral posterior thalamic nucleus, mediocaudal; LPMR, lateral posterior thalamic nucleus, mediorostral; PLi, posterior limitans thalamic nucleus; PoT, posterior thalamic nuclear group, triangular; VPL, ventral posterolateral thalamic nucleus; VPM, ventral posteromedial thalamic nucleus. (**e**) Graphic representation of the dorso-ventral localization of the neurons shown in **d**. Color coding is as in **d**. (**f**–**j**) Examples of delayed and immediate photoactivation of individual dura-sensitive thalamic neurons by 50,000 (**f**,**g**), 3,000 (**h**,**i**) and 500 lx (**j**) of white light (green line). Window discriminator spike output (top) and mean activity histogram (bottom) are shown in **f** and **g**. Mean activity histograms are shown in **h** and **j**. Window discriminator output (top) and oscillographic tracing (bottom) are shown in **i**. Each of the light intensities induced delayed activation in some neurons (**f**,**h**,**j**) and immediate activation in others (**g**,**i**). Each of the light intensities induced prolonged activation that outlasted the stimulus by several minutes. The numbers in parentheses indicate mean spikes per s for the corresponding interval. Black and red bars indicate, respectively, baseline and enhanced periods of activity in response to light. Bin widths are 0.5 (**f**,**g**,**j**) and 1 s (**h**).

activation in three units (<1 s). Latencies for rapid activation with 50,000 and 500 lx could not be measured at millisecond resolution, as the light source was not synchronized with the data acquisition software. The wide range of response latencies led us to evaluate the anatomical relationships between retinal afferents and individual dura-sensitive neurons in the posterior thalamus.

Retinal afferents to thalamic dura/light-sensitive units

Retinal afferents were traced anterogradely by injecting 6 µl of 1% CTB into the vitreous body of one eye under brief isoflurane anesthesia. We identified individual dura/light-sensitive neurons (one neuron per rat) in the contralateral posterior thalamus 3 d later using a recording glass micropipette (20 MΩ) under extended isoflurane anesthesia. A neuron thus identified was then filled with the anterograde tracer tetramethylrhodamine-dextran conjugate (TMR-dextran), which was preloaded into the recording micropipette. Juxtacellular iontophoresis of the tracer into the target neuron was performed over a period of 10–60 min by synchronizing neuronal firing with a 1–10-nA positive current delivered in a train of 200-ms on/off intervals (**Fig. 3a**).

In the four cases of successful double labeling (U1–U4; **Fig. 3b**), boutons along retinal afferents were present in apposition to dendrites and/or the cell body of the dura/light-sensitive unit (**Fig. 3c** and **Supplementary Fig. 6**). Neuronal responses to light (**Fig. 3d**) were of short latency (240 ms), short duration (35 s) and large magnitude (17 spikes per s) in U1, long latency (6–8 s), long duration (>100 s) and small magnitude (<5 spike per s) in U2 and U3, and long latency (10.5 s), short duration (13 s) and small magnitude in U4.

Cortical projections of dura/light-sensitive units

The final experiment was aimed at visualizing and mapping the axonal projections of individual thalamic neurons that were identified electrophysiologically as dura/light-sensitive units and filled juxtacellularly with TMR-dextran (**Fig. 4a**). In each case, the parent axon projected ipsilaterally through the thalamic reticular nucleus, where it issued a dense collateral terminal field (**Fig. 4b**), and ascended rostrally through caudate putamen into the external capsule (**Fig. 4b**,**c**). The parent axons looped backward in the external capsule, sending branches into multiple cortical regions (**Fig. 4d**–**f**). These included the primary somatosensory cortex, primary somatosensory barrel field, primary somatosensory trunk region, primary somatosensory dysgranular region, the primary and secondary motor cortices, the retrosplenial agranular cortex, the parietal association cortex, the binocular area of the primary visual cortex, and the lateral and mediolateral areas of the secondary visual cortex. Axonal branches in each cortical target extended across layers I through V (**Fig. 4d**–**f**).

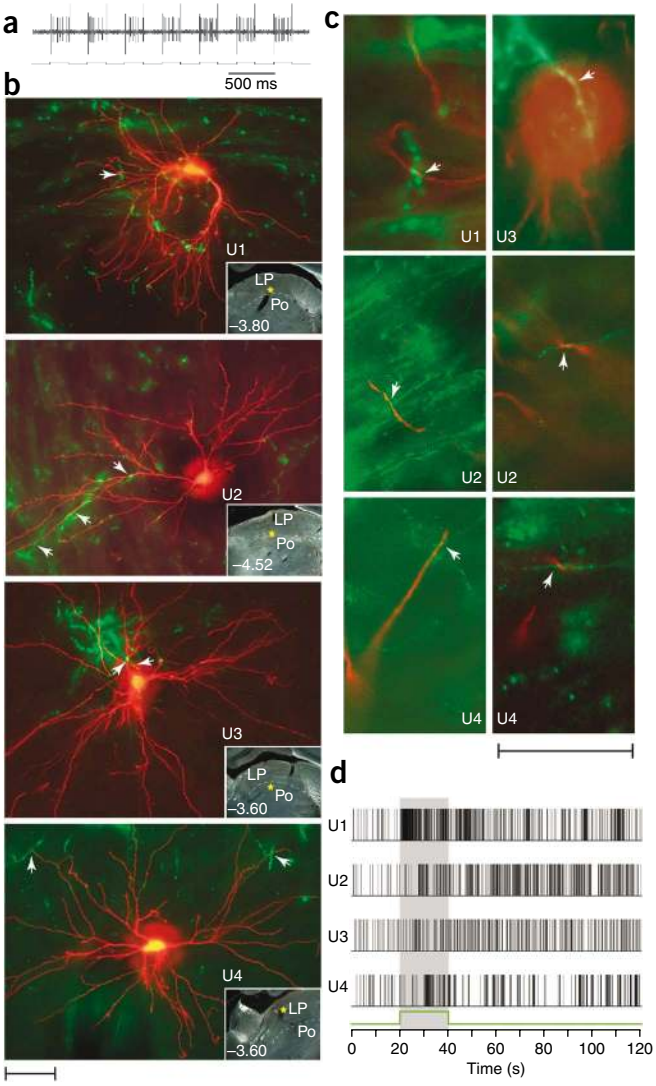

Figure 3 Close apposition between dura/light-sensitive neurons and retinal afferents in lateral posterior thalamic nuclei and posterior thalamic nuclear group. (**a**) Synchronization of neuronal activity (top) with the current (bottom) delivered by the TMR-dextran–filled recording micropipette. (**b**) Dura/light-sensitive units (U1–U4) filled with TMR-dextran (red) and retinal axons labeled anterogradely with CTB (green). Each image represents *z* stacking of approximately 30 1–1.5-μm-thick scans. Arrowheads point to potential axodendritic or axosomatic apposition. Localization of each cell body is marked by a yellow star in the low-power, darkfield inset. The numbers indicate distance from bregma. (**c**) Evidence for axodendritic and axosomatic apposition in a single 1–1.5-μm-thick scan taken from the units shown in **b**. (**d**) Neuronal firing in response to 50,000 lx of white light (green line and shaded area), corresponding to the individual neurons shown in **b**. Scale bars represent 50 μm (**b**,**c**).

DISCUSSION

Our findings reveal a mechanism for the exacerbation of migraine headache by light, whereby the neuronal activity of a nociceptive pathway that underlies migraine pain (**Supplementary Fig. 7**) is modulated at the level of the thalamus by retinal photoactivation. We propose that this photomodulation is exerted by axonal projections of RGCs that converge on dura-sensitive neurons in a discrete area in the posterior thalamus (**Supplementary Fig. 7**). To a large extent, the retinal projections to the posterior region of the thalamus consisted of axons of ipRGCs (**Fig. 1** and **Supplementary Fig. 4**), which have been shown to be important in a growing number of non–image-forming functions[17,19–25]. The idea that ipRGCs are involved in migraine photophobia is supported by our finding that exacerbation of migraine headache by light was preserved in blind individuals who could sense light in the face of severe degeneration of rod and cone photoreceptors. Our mapping of the axonal projections of dura-sensitive thalamic neurons unravels for the first time, to the best of our knowledge, the cortical terminal fields of the trigeminovascular pathway.

In migraine patients with normal eyesight, exacerbation of headache by light is likely to involve both extrinsic photoactivation of ipRGCs by rods and cones, as well as intrinsic photoactivation of melanopsin[34,35]. The presence of migraine photophobia in blind patients with outer retinal degeneration was associated with the preservation of PLR and circadian photoentrainment, suggesting that non–image-forming pathways remained intact in these individuals. Indeed, histological examination of eyes from retinitis pigmentosa patients with total loss of outer photoreceptor layer demonstrated preservation of the melanopsin-expressing ipRGC inner layer[36]. In the case of our photosensitive blind subjects, we cannot rule out the possibility that certain aspects of nonvisual functions are mediated by functioning rods and cones that survived the retinal disease.

The retinal projection to lateral posterior thalamic nuclei and the posterior thalamic nuclear group is distinct from the main visual pathway. This projection appeared to be similar in cases in which a large intravitreal injection of rAAV-GFP produced dense labeling along all known visual pathways and in cases in which a small injection produced preferential labeling in the suprachiasmatic nucleus, IGL and OPT, structures that subserve non–image-forming functions[22–25]. As 80% of RGCs labeled by the small injection of the tracer expressed melanopsin[22], we conclude that the retinal projections that we observed in the posterior thalamus originated to a large extent in ipRGCs and to a lesser extent in non-melanopsinergic RGCs.

The photosensitivity of dura-sensitive units in the rat thalamus consisted of short (<1 s) or long (>1 s) response latencies, prolonged discharges and slow decay of activity. To a limited degree, an instantaneous surge of firing in response to light may be attributed to activation of RGCs and ipRGCs by rods and cones, whereas subsequent long-lasting activity that subsides slowly in the dark may be attributed to ipRGC signals that are driven intrinsically by melanopsin photoactivation[28,35,37,38]. Photoactivation of dura-sensitive thalamic neurons inside of hundreds of milliseconds may be consistent with monosynaptic input from RGCs triggered by rods and cones. This possibility may be further supported by the close apposition between dura/light-sensitive neurons and boutons of retinal axons in lateral posterior thalamic nuclei and posterior thalamic nuclear group observed in 1–1.5-μm-thick scans (**Fig. 3c**). The number and nature of such close appositions at the level of a distal dendrite, proximal dendrite or cell body (**Fig. 3b**) may influence the probability of firing in response to light by individual lateral posterior thalamic nuclei/posterior thalamic nuclear group neurons, including response latency, magnitude and duration (**Fig. 3d**). It should be emphasized, however, that the intrinsic ongoing activity of dura-sensitive thalamic neurons and the input that they continue to receive from the meninges may mask the onset of their activation by light and confound the relative contribution of RGCs or ipRGCs to their response duration and response decay.

The instantaneous induction of neuronal firing in response to light and its slow decay in the dark may be consistent with the

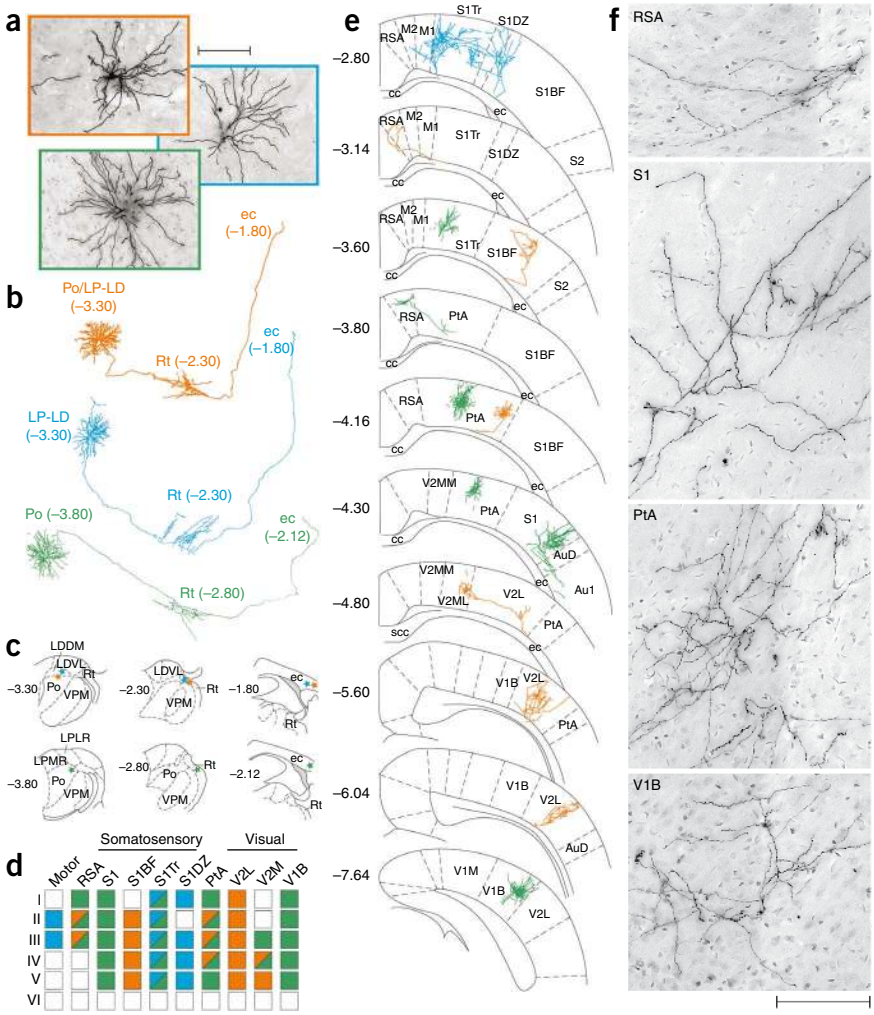

Figure 4 Cortical projections of three dura/light-sensitive thalamic neurons juxtacellularly filled with TMR-dextran. (**a**) Labeled cell bodies and their dendrites in the posterior thalamus. (**b**) Camera-lucida tracing of the cell bodies, dendrites and axonal trajectories coursing through thalamic reticular nucleus (Rt) en route the external capsule (ec). (**c**) Localization of cell bodies, Rt collaterals and entry point of the parent axon into the external capsule. (**d**) Tabulation of cortical areas and layers containing axons with synaptic boutons. PtA, parietal association cortex; RSA, retrosplenial agranular cortex; S1, primary somatosensory cortex; S1BF, primary somatosensory barrel field; S1Tr, primary somatosensory trunk region; S1DZ, primary somatosensory dysgranular region; V1B, binocular area of the primary visual cortex; V2L and V2M, lateral and mediolateral areas of the secondary visual cortex, respectively. (**e**) Camera-lucida tracing of axon terminal fields in different cortical areas. Au1, primary auditory cortex; AuD, secondary auditory cortex, dorsal; M1 and M2, primary and secondary motor cortices, respectively. (**f**) Photomicrographs of axons with synaptic boutons in several cortical areas. Drawings and numbers (**b**,**c**,**e**) indicating distance from bregma (mm) are based on ref. 46. Scale bars represent 100 μm (**a**,**f**). LDDM, laterodorsal thalamic nucleus, dorsomedial.

exacerbation of migraine headache by light and its slow relief in the dark. Most photosensitive blind migraineurs and those with normal eyesight testified that headache severity increased within a few seconds of light exposure and decreased over 10–20 min after return to a dark environment (**Supplementary Table 1**). Photoactivation of dura-sensitive thalamic units that was delayed by several minutes might be consistent with the delayed exacerbation of migraine headache by light reported by some individuals (**Supplementary Table 1**) but cannot be explained at this juncture vis-à-vis the response properties of RGCs.

To the best of our knowledge, this is the first study to map out the cortical terminal fields of the trigeminovascular pathway. Anterograde transport of tritiated amino acids from the posterior thalamic nuclear group to axons in S1 has been traced only to layers I and V[39]. We identified singularly labeled dura-sensitive thalamic neurons that form widespread axonal terminal fields spanning layers I–V of the barrel field and trunk region of the primary somatosensory cortex. Although it is generally accepted that the primary somatosensory cortex is involved in certain aspects of the experience of pain[40], its role in processing migraine headache remains to be determined. Additional projections to cortical areas involved in cognitive, motor and visual functions may mediate a number of transient symptoms associated with migraine, such as loss of short-term memory (retrosplenial cortex[41]), muscle weakness and impaired motor coordination (motor cortex[42]), attention deficits (parietal association cortex[43]), and visual disturbances (visual cortex[44,45]).

METHODS

Methods and any associated references are available in the online version of the paper at http://www.nature.com/natureneuroscience/.

Note: Supplementary information is available on the Nature Neuroscience website.

ACKNOWLEDGMENTS

We thank D. Friedman, A. Recober, M. Carmen-Wilson and A. Mauskop for sharing their blind migraine patients, and L. Villanueva and J.-F. Bernard for teaching us the juxtacellular labeling technique. This research was supported by US National Institutes of Health grants NS-051484 and NS-035611. K.D. was supported in part by an unrestricted grant from Research to Prevent Blindness.

AUTHOR CONTRIBUTIONS

R.B., M.J. and R.N. designed the study. R.N., V.K., J.J.G. and R.B. conducted the various experiments. M.J., R.N., C.B.S. and K.D. contributed to data analysis and presentation. R.B. and M.J. wrote the manuscript.

COMPETING INTERESTS STATEMENT

The authors declare no competing financial interests.

Published online at http://www.nature.com/natureneuroscience/.
Reprints and permissions information is available online at http://www.nature.com/reprintsandpermissions/.

1. Headache Classification Subcommittee of the International Headache Society. The international classification of headache disorders: second edition. *Cephalalgia* **24**, 9–160 (2004).
2. Selby, G. & Lance, J.W. Observations on 500 cases of migraine and allied vascular headache. *J. Neurol. Neurosurg. Psychiatry* **23**, 23–32 (1960).
3. Markowitz, S., Saito, K. & Moskowitz, M.A. Neurogenically mediated plasma extravasation in dura mater: effect of ergot alkaloids. A possible mechanism of action in vascular headache. *Cephalalgia* **8**, 83–91 (1988).

4. Penfield, W. & McNaughton, F. Dural headache and innervation of the dura mater. *Arch. Neurol. Psychiatry* **44**, 43–75 (1940).
5. Burstein, R., Yamamura, H., Malick, A. & Strassman, A.M. Chemical stimulation of the intracranial dura induces enhanced responses to facial stimulation in brain stem trigeminal neurons. *J. Neurophysiol.* **79**, 964–982 (1998).
6. Strassman, A.M., Raymond, S.A. & Burstein, R. Sensitization of meningeal sensory neurons and the origin of headaches. *Nature* **384**, 560–564 (1996).
7. Burstein, R., Yarnitsky, D., Goor-Aryeh, I., Ransil, B.J. & Bajwa, Z.H. An association between migraine and cutaneous allodynia. *Ann. Neurol.* **47**, 614–624 (2000).
8. Burstein, R., Cutrer, F.M. & Yarnitsky, D. The development of cutaneous allodynia during a migraine attack: clinical evidence for the sequential recruitment of spinal and supraspinal nociceptive neurons in migraine. *Brain* **123**, 1703–1709 (2000).
9. Kawasaki, A. & Purvin, V.A. Photophobia as the presenting visual symptom of chiasmal compression. *J. Neuroophthalmol.* **22**, 3–8 (2002).
10. Liveing, E. *On Megrim, Sick Headache* (Arts & Boeve Publishers, Nijmegen, The Netherlands, 1873).
11. Lebensohn, J.E. Photophobia: mechanism and implications. *Am. J. Ophthalmol.* **34**, 1294–1300 (1951).
12. Aurora, S.K., Cao, Y., Bowyer, S.M. & Welch, K.M. The occipital cortex is hyperexcitable in migraine: experimental evidence. *Headache* **39**, 469–476 (1999).
13. Lamonte, M., Silberstein, S.D. & Marcelis, J.F. Headache associated with aseptic meningitis. *Headache* **35**, 520–526 (1995).
14. Welty, T.E. & Horner, T.G. Pathophysiology and treatment of subarachnoid hemorrhage. *Clin. Pharm.* **9**, 35–39 (1990).
15. Lowenfeld, I. *The Dazzling Syndrome* (Wane State University Press, Detroit, Michigan, USA, 1993).
16. Miller, N.R. Photophobia. in *Walsh and Hoyt's Clinical Neuro-ophthlmology* (ed. N.R. Miller) 1099–1106 (Williams & Wilkins, Baltimore, 1985).
17. Lucas, R.J., Douglas, R.H. & Foster, R.G. Characterization of an ocular photopigment capable of driving pupillary constriction in mice. *Nat. Neurosci.* **4**, 621–626 (2001).
18. Klein, D.C. & Weller, J.L. Rapid light-induced decrease in pineal serotonin N-acetyltransferase activity. *Science* **177**, 532–533 (1972).
19. Freedman, M.S. *et al.* Regulation of mammalian circadian behavior by non-rod, non-cone, ocular photoreceptors. *Science* **284**, 502–504 (1999).
20. Hattar, S. *et al.* Melanopsin and rod-cone photoreceptive systems account for all major accessory visual functions in mice. *Nature* **424**, 76–81 (2003).
21. Lucas, R.J., Freedman, M.S., Munoz, M., Garcia-Fernandez, J.M. & Foster, R.G. Regulation of the mammalian pineal by non-rod, non-cone, ocular photoreceptors. *Science* **284**, 505–507 (1999).
22. Gooley, J.J., Lu, J., Fischer, D. & Saper, C.B. A broad role for melanopsin in nonvisual photoreception. *J. Neurosci.* **23**, 7093–7106 (2003).
23. Güler, A.D. *et al.* Melanopsin cells are the principal conduits for rod-cone input to non-image-forming vision. *Nature* **453**, 102–105 (2008).
24. Hattar, S. *et al.* Central projections of melanopsin-expressing retinal ganglion cells in the mouse. *J. Comp. Neurol.* **497**, 326–349 (2006).
25. Hannibal, J. & Fahrenkrug, J. Target areas innervated by PACAP-immunoreactive retinal ganglion cells. *Cell Tissue Res.* **316**, 99–113 (2004).
26. Provencio, I., Jiang, G., De Grip, W.J., Hayes, W.P. & Rollag, M.D. Melanopsin: An opsin in melanophores, brain and eye. *Proc. Natl. Acad. Sci. USA* **95**, 340–345 (1998).
27. Provencio, I. *et al.* A novel human opsin in the inner retina. *J. Neurosci.* **20**, 600–605 (2000).
28. Berson, D.M., Dunn, F.A. & Takao, M. Phototransduction by retinal ganglion cells that set the circadian clock. *Science* **295**, 1070–1073 (2002).
29. Hattar, S., Liao, H.W., Takao, M., Berson, D.M. & Yau, K.W. Melanopsin-containing retinal ganglion cells: architecture, projections, and intrinsic photosensitivity. *Science* **295**, 1065–1070 (2002).
30. Panda, S. *et al.* Melanopsin is required for non-image-forming photic responses in blind mice. *Science* **301**, 525–527 (2003).
31. Malick, A., Jakubowski, M., Elmquist, J.K., Saper, C.B. & Burstein, R. A neurohistochemical blueprint for pain-induced loss of appetite. *Proc. Natl. Acad. Sci. USA* **98**, 9930–9935 (2001).
32. Zagami, A.S. & Lambert, G.A. Stimulation of cranial vessels excites nociceptive neurones in several thalamic nuclei of the cat. *Exp. Brain Res.* **81**, 552–566 (1990).
33. Davis, K.D. & Dostrovsky, J.O. Properties of feline thalamic neurons activated by stimulation of the middle meningeal artery and sagittal sinus. *Brain Res.* **454**, 89–100 (1988).
34. Dacey, D.M. *et al.* Melanopsin-expressing ganglion cells in primate retina signal colour and irradiance and project to the LGN. *Nature* **433**, 749–754 (2005).
35. Wong, K.Y., Dunn, F.A., Graham, D.M. & Berson, D.M. Synaptic influences on rat ganglion-cell photoreceptors. *J. Physiol. (Lond.)* **582**, 279–296 (2007).
36. Hannibal, J. *et al.* Melanopsin is expressed in PACAP-containing retinal ganglion cells of the human retinohypothalamic tract. *Invest. Ophthalmol. Vis. Sci.* **45**, 4202–4209 (2004).
37. Berson, D.M. Phototransduction in ganglion-cell photoreceptors. *Pflugers Arch.* **454**, 849–855 (2007).
38. Tu, D.C. *et al.* Physiologic diversity and development of intrinsically photosensitive retinal ganglion cells. *Neuron* **48**, 987–999 (2005).
39. Herkenham, M. Laminar organization of thalamic projections to the rat neocortex. *Science* **207**, 532–535 (1980).
40. Ingvar, M. & Hsieh, J.-C. The image of pain. in *Textbook of Pain* (eds P.D. Wall & R. Melzack) 215–233 (Churchill Livingston, London, 1999).
41. Valenstein, E. *et al.* Retrosplenial amnesia. *Brain* **110**, 1631–1646 (1987).
42. Donchin, O., Gribova, A., Steinberg, O., Bergman, H. & Vaadia, E. Primary motor cortex is involved in bimanual coordination. *Nature* **395**, 274–278 (1998).
43. Mountcastle, V.B., Lynch, J.C., Georgopoulos, A., Sakata, H. & Acuna, C. Posterior parietal association cortex of the monkey: command functions for operations within extrapersonal space. *J. Neurophysiol.* **38**, 871–908 (1975).
44. Lowel, S. & Singer, W. Selection of intrinsic horizontal connections in the visual cortex by correlated neuronal activity. *Science* **255**, 209–212 (1992).
45. Livingstone, M.S. & Hubel, D.H. Anatomy and physiology of a color system in the primate visual cortex. *J. Neurosci.* **4**, 309–356 (1984).
46. Paxinos, G. & Watson, C. *The Rat Brain in Stereotaxic Coordinates* (Academic Press, Orlando, Florida, USA, 1998).

ONLINE METHODS

Animal and human subjects. Studies were conducted in accordance with US National Institutes of Health guideline and were approved by the Institutional Animal Care and Use Committee and Committee on Clinical Investigations of Beth Israel Deaconess Medical Center. We recruited 12 blind migraineurs nationwide through their headache specialists and interviewed them in person. An additional eight individuals were interviewed by phone after responding to national and international announcements disseminated electronically and in print newsletters and magazines serving blind and visually impaired individuals. The interview covered general medical, migraine and visual history, characteristics of migraine attacks and associated symptoms, and visual and nonvisual photoperception in the presence and absence of migraine. Diagnoses of migraine and visual condition were determined by neuro-ophthalmologist/headache specialists using information gathered in the interview and available medical charts.

Single-unit recording. Single-unit recording, including surgical preparation and criteria for neuronal responses, were performed as described previously[47,48]. A recording microelectrode was lowered slowly into the posterior thalamus while searching for single-unit responses to repetitive electrical pulses (0.8 ms, 0.5–3.0 mA, 1 Hz), which were applied to the dura through a bipolar electrode at the contralateral transverse sinus. The experiments shown in **Figure 2** were performed under deep urethane anesthesia (1.5 g per kg of body weight, intraperitoneal) using stainless-steel recording electrodes (1–4 MΩ). The experiments shown in **Figures 3** and **4** were performed under isoflurane anesthesia (initially induced with 5%, reduced to 2% during the preparatory surgery and maintained at 1–1.2% later on) using glass micropipettes (20 MΩ). Neurons responding to electrical pulses were selected if they also responded to indentation of the dura with calibrated von-Frey monofilament and to chemical stimulation of the dura with gelfoam soaked with 1 M KCl. Such dura-sensitive units were tested for photosensitivity by monitoring their ongoing activity in the dark for 10 min before and for 10 min after a 10-s episode of bright light (50,000 lx). Units responding to bright light were also tested with lower light intensities (500 or 3,000 lx). A neuron was classified as photosensitive if its mean rate of firing was 25% greater under 500 lx than in the dark. At the end of each experiment (one neuron per rat), an electrolytic lesion marking the recording site was produced by passing direct anodal current (20 μA for 20 s) through the tip of the electrode. Histological localization of the recording site was determined using microscopic examination of serial coronal sections of the brain.

Colabeling of retinal afferents and dura/light-sensitive neurons. Retinal afferents were traced anterogradely by injecting 6 μl of 1% CTB into the vitreous body of one eye[22] under brief isoflurane anesthesia. Dura/light-sensitive neurons were identified 3 d later using single-unit recording in the contralateral posterior thalamus (one neuron per rat) and filled with 3% TMR-dextran (wt/vol, 3,000 molecular weight, anionic, lysine fixable; D-3308, Invitrogen). This was done under deep isoflurane anesthesia using a procedure of juxtacellular iontophoresis (**Fig. 3a**), described previously[49,50]. Isoflurane anesthesia was replaced 4 h later with deep pentobarbital anesthesia (50 mg per kg, intraperitoneal) and each rat was killed by transcardiac perfusion with 200 ml of heparinized saline, followed by 500 ml of 4% paraformaldehyde (wt/vol) and 0.05% picric acid (wt/vol), in 0.1 M phosphate-buffered saline (PBS). Brains were removed from the skull, kept in the fixative solution for 2 h and cryoprotected in 30% sucrose (wt/vol) phosphate buffer for 48 h. Brains were then frozen and cut into serial coronal sections (80 μm thick) using a cryostat (Leica).

For immunolabeling of CTB, free-floating brain sections were pre-incubated for 1 h with 0.1 M PBS containing 0.25% Triton X-100 (wt/vol), incubated for 48 h at 4 °C with goat primary antibody to CTB (1:50,000 dilution, List Biological Labs) and incubated for 2–3 h at 22–25 °C with donkey secondary antibody to goat conjugated with Alexa Fluor 488 (1:500 dilution, Invitrogen). Each step was preceded and followed by washes in 0.1 M PBS. Digital imaging was performed using fluorescent light (Leica) or confocal (Zeiss) scanning microscopy that compiled 1–1.5-μm-thick scans using *z* stacking software. Retinal afferents immunolabeled with Alexa Fluor 488 were detected by excitation at 455 nm and emission at 520 nm (green). Neurons labeled with TMR-dextran were detected in the same set of sections by excitation at 551 nm and emission at 624 nm (red). Colabeling of the two anterograde tracers was achieved by superimposition of the green and red images (**Fig. 3b**,**c** and **Supplementary Fig. 5**).

Mapping of axonal projections of dura/light-sensitive neurons. Dura/light-sensitive thalamic neurons were identified using single-unit recording and filled with TMR-dextran under isoflurane anesthesia as described above. The rats were killed by perfusion with fixative solution 3 d later and their brains were removed, cryoprotected and cut into sections as described above. Free-floating sections were pretreated for 1 h at 22–25 °C with 3:1 methanol/PBS solution containing 1% H_2O_2 (wt/vol), pre-incubated for 1 h at 22–25 °C in antibody-dilution solution (PBS containing 2% fetal serum albumin (wt/vol), 0.3% Triton X-100), incubated for 48 h at 4 °C with rabbit primary antibody to TMR (1:3,000 dilution, Invitrogen), incubated with biotinylated goat secondary antibody to rabbit (1:500 dilution, Jackson ImmunoResearch Labs), processed for 2 h with avidin-biotin complex kit (Vector Labs) and detected using nickel-enhanced 3,3′-diaminobenzidine. Each step was preceded and followed by washes in 0.1 M PBS. Immunostained sections were mounted on glass slides, counterstained with thionin and coverslipped. The cell body, dendrites, parent axon and cortical axonal branches of each injected neuron (spanning 20, 36 or 50 consecutive coronal sections per brain) were penciled in aggregate using brightfield microscopy and the camera lucida technique (**Fig. 4b**,**c**,**e**).

Retrograde tracing of afferent projections to the posterior thalamus. The cell bodies of neurons projecting to the posterior thalamic nuclear group were mapped using the retrograde tracer Fluorogold (hydroxystilbamidine, Interchim). A glass micropipette (50-μm tip diameter) loaded with 2% Fluorogold (wt/vol) solution was lowered into the dorsal part of the rat posterior thalamic nuclear group under deep isoflurane anesthesia. Iontophoretic release of the tracer was achieved by delivering direct positive current (5–10 μA, on-off cycles, 10 s per cycle) over 10–15 min. After a 4-d recovery period, rats were perfused with fixative solution and the brain, along with the eyeballs and an upper cervical segment of the spinal cord, was cryoprotected and frozen as described above. Serial coronal sections were collected from the brain and spinal cord (40 μm thick) and from the eyeballs (25 μm thick), mounted on glass slides, and coverslipped. The injection site and retrograde-labeled cell bodies containing Fluorogold were visualized by excitation at 360 nm and emission at 408 nm (blue) using fluorescence microscopy (Leica). Retrograde-labeled neurons were mapped in the medullary dorsal horn and in C1–C5 using camera lucida tracing (**Supplementary Fig. 3**). To test whether the retrograde-labeled RGCs included ipRGC units, we repeated the iontophoretic injection of Fluorogold in the posterior thalamic nuclear group described above and processed whole-retina preparations of both eyes for melanopsin immunoreactivity, using rabbit primary antibody against rat melanopsin (1:1,000 dilution, Thermo Scientific) and donkey secondary antibody to rabbit conjugated with Alexa Fluor 594 (1:400 dilution, Invitrogen). Immunostained ipRGC units were detected by fluorescence microscopy using excitation at 551 nm and emission at 618 nm (red). Colocalization of melanopsin and Fluorogold was achieved by superimposition of the red and blue images (**Supplementary Fig. 4**).

Statistical analysis. Rates of neuronal firing were compared between dark and light using Wilcoxon matched-pairs signed-ranks test with a two-tailed level of significance set at $\alpha = 0.05$.

47. Burstein, R. & Jakubowski, M. Analgesic triptan action in an animal model of intracranial pain: a race against the development of central sensitization. *Ann. Neurol.* **55**, 27–36 (2004).
48. Yamamura, H., Malick, A., Chamberlin, N.L. & Burstein, R. Cardiovascular and neuronal responses to head stimulation reflect central sensitization and cutaneous allodynia in a rat model of migraine. *J. Neurophysiol.* **81**, 479–493 (1999).
49. Pinault, D. A novel single-cell staining procedure performed in vivo under electrophysiological control: Morpho-functional features of juxtacellularly labeled thalamic cells and other central neurons with biocytin or Neurobiotin. *J. Neurosci. Methods* **65**, 113–136 (1996).
50. Gauriau, C. & Bernard, J.F. Posterior triangular thalamic neurons convey nociceptive messages to the secondary somatosensory and insular cortices in the rat. *J. Neurosci.* **24**, 752–761 (2004).

doi:10.1038/nn.2475